Journal of Instrumentation

TECHNICAL REPORT

Design study of a single bunch selection method for neutron TOF experiment at RAON heavy ion accelerator

To cite this article: S.H. Moon *et al* 2022 *JINST* **17** T07007

Published by IOP Publishing for Sissa Medialab

Received: *March 14, 2022*
Revised: *April 29, 2022*
Accepted: *June 7, 2022*
Published: *July 18, 2022*

TECHNICAL REPORT

Design study of a single bunch selection method for neutron TOF experiment at RAON heavy ion accelerator

S.H. Moon,[a,1] J.Y. Jeong,[a,1] D. Kwak,[a] J.H. Jang,[b] K.-B. Chai[c] and M. Chung[a,*]

[a] *Department of Physics, Ulsan National Institute of Science and Technology, Ulsan 44919, Republic of Korea*
[b] *Rare Isotope Science Project, Institute for Basic Science, Daejeon 34047, Republic of Korea*
[c] *Korea Atomic Energy Research Institute, Daejeon 34057, Republic of Korea*

E-mail: mchung@unist.ac.kr

Abstract: To enable neutron time-of-flight (TOF) experiments at the RAON heavy-ion accelerator facility, we propose a single bunch beam selection method by combining a fast chopper and double gap buncher in the low-energy beam transport (LEBT) section. The fast chopper operates with switching times of tens of ns to convert a CW beam into a pulsed beam. Then, the double gap buncher performs bunching to shorten the beam pulse duration to less than one radio frequency quadrupole (RFQ) cycle. Ideally, a single isolated bunch can be achieved after the RFQ. In this study, we discuss the system design of the proposed single bunch selection scheme and present detailed beam dynamics simulations.

Keywords: Accelerator modelling and simulations (multi-particle dynamics, single-particle dynamics); Accelerator Subsystems and Technologies; Beam dynamics; Instrumentation for heavy-ion accelerators

[1] These authors contributed equally to this work.
[*] Corresponding author.

https://doi.org/10.1088/1748-0221/17/07/T07007

Contents

1 Introduction

Accelerator-based neutron sources generate neutrons through collisions between the accelerated beams and target material. Therefore, repetition rate of the neutron generation is dependent on the time structure of the beam. If a CW accelerator is used for neutron generation, the beam repetition time usually ranges from a few to tens of ns following the frequency of accelerating cavity. However, such a repetition time is too short for high-resolution neutron time-of-flight (TOF) experiments. To address this issue, several single bunch selection methods have been proposed [1–7]. The Soreq Applied Research Accelerator Facility (SARAF) proposed and tested a scheme based on a fast chopper [1, 2]. Therein, a CW beam is chopped into a pulsed beam in the low-energy beam transport (LEBT) region by varying the electric potential of the chopper electrode in a very short time ($\sim$ 28 ns). Then, the short-pulsed beam enters the radio frequency quadrupole (RFQ) and becomes a single bunch through the bunching process of RFQ. Successful single bunch selection characteristics with neighboring bunch contamination of less than 15% were reported [2]. The Grand Accélérateur National d'Ions Lourds (GANIL) suggested a single bunch selection method in the medium-energy beam transport (MEBT) region based on the compensation between electric and magnetic forces. Mostly the bending magnet diverts beam bunches into a dump. When a specific beam bunch needs to be transported downstream, short electric pulses are applied to meander electrodes and cancel the magnetic force from the bending magnet. Recently, GANIL team reported the experiment results, and the rate of satellite bunch was under 10^{-3} [3, 7]. The Tokai Radioactive Accelerator Complex (TRIAC) tested a single bunch selection technique combining a multi-layer chopper and a double gap buncher (DGB). Therein, a short-pulsed beam is first made by a multi-layer chopper. Then, the chopped beam enters the DGB. The DGB provides bunching to make the beam pulse shorter than one RFQ cycle. After the RFQ acceleration, the chopped beam becomes a single bunch. It was reported [4] that the beam loss at the multi-layer chopper was around 15% and the rate of satellite bunch was 10%.

These methods were successfully tested for various TOF experiments. For the RAON heavy-ion accelerator facility in Korea, similar TOF experiments are planned [8, 9]. Implementing the above mentioned single bunch selection methods on the RAON has been considered. To apply SARAF's method [1, 2], the length of the pulsed beam must be reduced at the RFQ entrance to avoid neighboring bunch contamination. The beam energy of SARAF is 20 keV/u, and the distance between the chopper and RFQ is approximately 1 m. Therefore, the length of the pulsed beam is not significantly increased during the drift. On the other hand, the beam energy of RAON is 10 keV/u, and the distance between the chopper and RFQ is approximately 4 m. Therefore, the length of the pulsed beam significantly increases throughout the transport line. The single bunch selector of GANIL uses compensation between the electric force from the high-voltage pulser and magnetic force from the dipole magnet [3, 7]. The high voltage pulser must provide an electric kick to the beam bunch without affecting the neighboring bunches. Therefore, a high voltage pulser must have rise/fall times of a few ns. Such an approach would be possible for proton and deuteron beams. However, it becomes very difficult for high A/q beams because the required voltage increases accordingly. The RAON plans to use a wide range of A/q beams, 1–7, for various TOF experiments. Therefore, GANIL's method is unfeasible or it would be costly for RAON. The combination of the multi-layer chopper and DGB, as used in the TRIAC, can be another choice. However, it is difficult to change the existing RAON chopper to a TRIAC-type multi-layer chopper owing to different operating conditions. Normally, the beam loss at the multi-layer chopper is unavoidable and is expected to be approximately 5% at TRIAC. In real experiment, the beam loss was reported to be approximately 14% because of the finite angular distribution of the beam [4]. The beam energy at the TRIAC LEBT is 2 keV/u, whereas it is 10 keV/u at the RAON LEBT. Therefore, the long-term operational stability of a multi-layer chopper system would be very uncertain for the higher beam power operation expected at the RAON.

To overcome this situation, we combined SARAF's fast chopper and TRIAC's DGB. We propose to fabricate a fast chopper by upgrading the electric components of the existing slow chopper at the RAON. The fast chopper and collimator generate a pulsed beam of hundreds of ns pulse length. Subsequently, the DGB performs bunching to shorten the pulse length less than one RFQ cycle. Ideally, we can get one single isolated bunch after the RFQ acceleration.

2 RAON LEBT, RFQ, and MEBT

The LEBT section of the RAON consists of two electron cyclotron resonance (ECR) ion sources and matching beamlines. One ECR ion source, which is presented on the left side of figure 1, is a superconducting ECR ion source and is designed to produce high A/q beams, such as a uranium ion beam. The other ECR is a normal conducting ECR ion source designed for low A/q beams, such as proton or deuteron beams. These ECR ion sources extract beams with 10 keV/u of energy. The extracted beam goes to the first 90° bending magnet for charge selection. The selected beam passes the T-shaped dipole and enters the RFQ-matching lattice.

The RFQ-matching beamline comprises several electrostatic quadrupoles (ESQs), a magnetic quadrupole (MQ), and a chopper. The chopper electrodes are installed after the electrostatic triplet which is placed after the T-shaped dipole. The installation position of the fast chopper does not

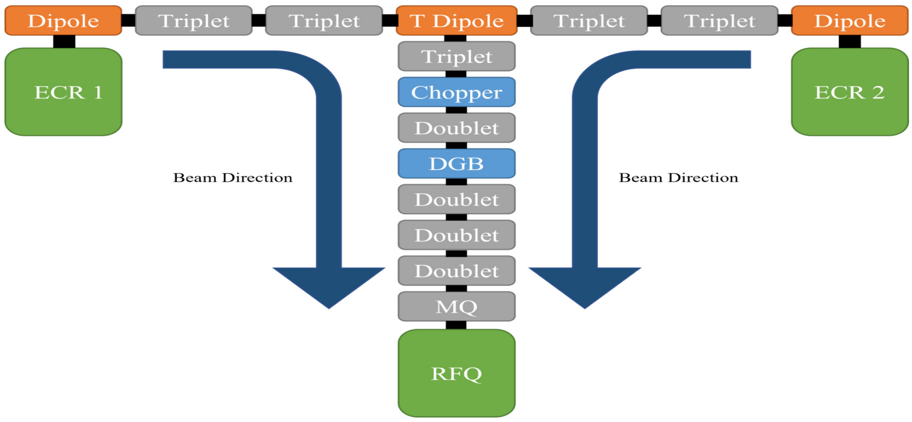

Figure 1. Schematic of the RAON LEBT section. The collimators are installed at the chopper vacuum chamber.

Figure 2. Picture of the RAON injector section. The DGB is placed at the earliest place where there is sufficient longitudinal space between the chopper and RFQ.

change because we only upgrade the electric components of the chopper. The DGB is placed between the first and second ESQ doublets. After the RFQ matching beamline, the beam enters the RFQ, which operates with 81.25 MHz. After the LEBT, the 10 keV/u beam enters the RFQ and is accelerated to 0.5 MeV/u at 81.25 MHz. Our goal is to put the pulsed beam within one RF cycle, thus, we aim to construct a beam with a pulse length less than 12.3 ns at the first RFQ cell.

The MEBT consists of 11 magnetic quadrupoles and four normal conducting re-bunchers. These quadrupoles and re-bunchers manipulate the beam for matching into superconducting quarter-wave resonator (QWR) accelerating cavities. In addition, four sets of wire scanners, six beam position monitors (BPMs), two normal Faraday cup and a fast Faraday cup are installed in the MEBT for beam diagnostics. To monitor whether the single bunch selection method works properly, we plan to use a direct BPM signal (similar to figure 9 of ref. [2]) and fast Faraday cup to check the time structure of the selected beam.

Figure 2 is the picture of the RAON injector section. The ECR 2 in figure 1 is placed at the left side of figure 2, which is blocked by shielding walls.

3 Basic parameter studies

In this parameter study, the main goals of the simulations are to determine the appropriate switching time and estimate the correlation between the chopper settings and properties of the selected beam pulse. The parameter study was conducted using the WARP particle-in-cell (PIC) simulation code [10]. Figure 3 shows the simulation results regarding the relationship between the switching time of the fast chopper and length of the selected beam pulse. Here, the beam species is Ar^{9+}, and the slit width is 8 mm with a 2.5 kV chopper voltage. The chopper has two parallel electrodes: the ground electrode and high voltage (HV) electrode.

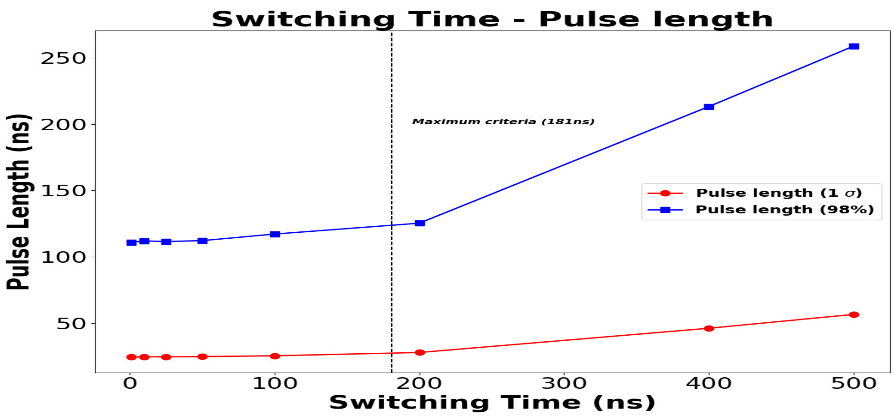

Figure 3. Pulse length after the collimator as a function of the chopper switching time.

The fast chopper perturbs the beam path transversely by switching the HV electrode potential from positive to negative or from negative to positive. The perturbed beam is dumped to the collimator and only the beam particles which have zero net kicks are transmitted to downstream. In this way, a CW beam is converted into a short pulsed beam. Therefore, for a proper operation of the collimator, the switching time must be shorter than the time required for the beam to pass through the chopper electrodes. The initial beam energy is 10 keV/u, which corresponds to a beam velocity of 1.38×10^6 m/s. Hence, for a chopper electrode length of 250 mm, the switching time should be less than 181 ns.

Figure 3 also shows that, if the switching time is longer than the maximum allowable value (181 ns), the pulse length of the selected beam dramatically increases. Once the switching time becomes shorter than approximately 100 ns, there is no significant reduction of the pulse length. Therefore, we aim to achieve a switching time of less than 100 ns considering the cost and technical difficulty in a fast high voltage switching circuit. Figure 4 shows the longitudinal phase space plots of the simulation cases considered in figure 3. If the switching time is shorter than 100 ns, the phase spaces show similar shapes. On the other hand, if the switching time is longer than 181 ns, the phase spaces start to change. Whereas the mean beam energy shifts are reduced, the pulse lengths become considerably longer.

The simulation results presented in figure 5 underline the relationship among the chopper voltage setting value, mean beam energy, and energy spread. Here, the chopper voltage varies from 2.5 to 5 kV. The optimal chopper voltage should be determined by considering the beam species and initial beam conditions, such as the RMS beam size. Thus, here we only discuss the mutual

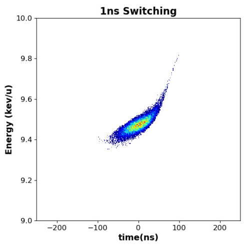

(a) 1 ns switching time.

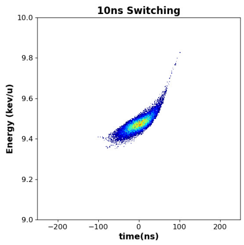

(b) 10 ns switching time.

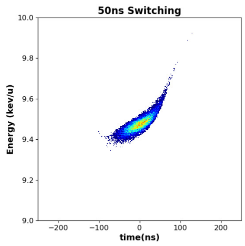

(c) 50 ns switching time.

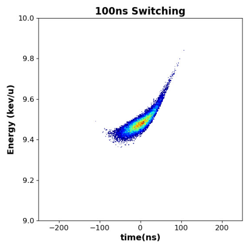

(d) 100 ns switching time.

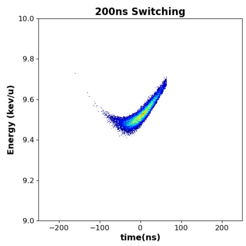

(e) 200 ns switching time.

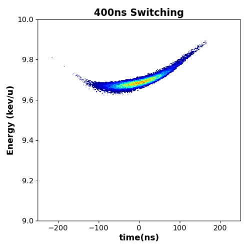

(f) 400 ns switching time.

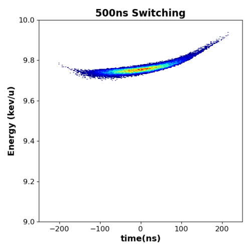

(g) 500 ns switching time.

Figure 4. Longitudinal phase spaces corresponding to the cases considered in figure 3.

dependency among the parameters. The simulation setting is the same as that used in figure 3, except for a switching time of 25 ns.

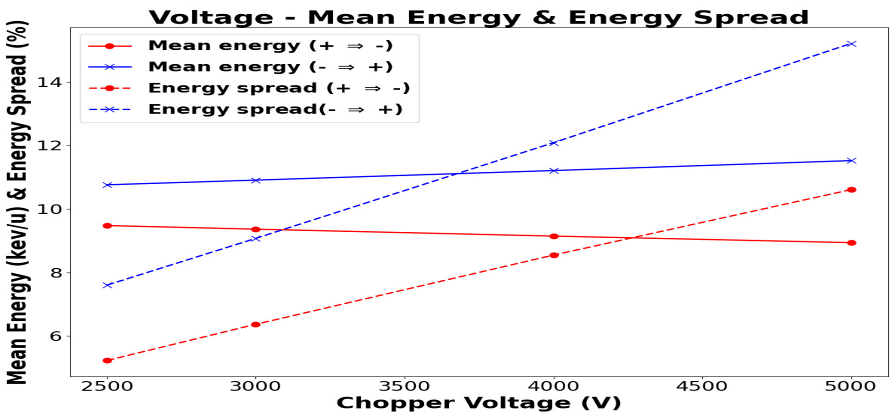

Figure 5. Mean beam energy and energy spread as a function of the chopper voltage. If the HV electrode voltage changes from positive (negative) to negative (positive), then the mean energy of the beam decreases (increases).

Two different scenarios are shown in figure 5. One is a simulation in which the chopper voltage changes from positive to negative, and the other is the opposite case. Normally, the beam energy does not change after passing through the chopper. For example, if the chopper HV electrode maintains a positive voltage, the beam decelerates at the chopper entrance and accelerates at the chopper exit. However, when the polarity of the HV electrode voltage is reversed during beam passage, the initially decelerated (accelerated) beam is decelerated (accelerated) again at the exit.

2022 JINST 17 T07007

This tendency is illustrated in figure 5. Note that the energy spread of the beam increases when the chopper voltage increases in both scenarios.

The last basic parameter study considers the relationship between the chopper voltage and length of the selected beam pulse. The simulation results are depicted in figure 6. As the chopper voltage

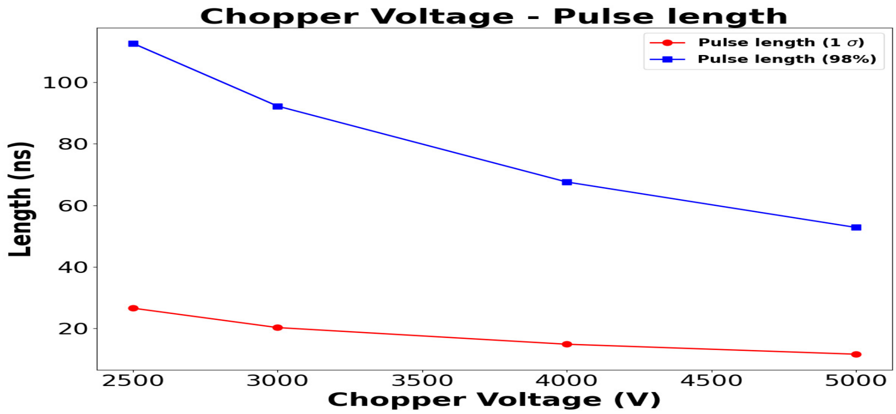

Figure 6. Pulse length as a function of the chopper voltage.

increases, the selected beam pulse becomes shorter. A shorter bunch length might be desirable; however, as shown in figure 5, a higher voltage introduces higher energy spread and mean energy shift. Such beam property changes can hinder RFQ matching. The RAON RFQ is designed for a 10 keV/u energy beam, and the RFQ transmission becomes worse for a larger energy spread of the initial beam. The DGB, installed after the chopper, can control the length of the selected beam pulse via the bunching process. However, the energy spread of the beam is not controllable after the chopper. Therefore, we plan to set the chopper voltage as low as possible in the actual beam experiment.

4 Beam dynamics simulation

Beam dynamics simulations are conducted for proton, deuteron, and argon beams. The simulation codes used in this study include WARP [10], TRACEWIN [11], and TRACK [12]. The WARP code is used for the fast chopper and collimator simulations, and the TRACEWIN code is used for the bunching and RFQ matching. Lastly, the TRACK code is used for RFQ simulation. The simulation starts from the endpoint of the ESQ triplet, which is placed after the T-shaped dipole. Detailed simulation settings are reported in table 1. Most setting parameters are kept identical between simulations, except the initial current and chopper voltage. A low A/q beam, such as a proton beam, is more vulnerable to space charge effects. Hence, for the proton beams, the initial beam current is set lower than that of the other beam species. The chopper voltage is increased according to the A/q value, which is set to 1000 V for the argon beam simulation. The chopper voltage setting depends on the initial beam parameters. For example, if there is a smaller RMS beam size at the chopper, the chopper voltage can be reduced. However, if the RMS beam size increases, a higher voltage must be used.

Figure 7 illustrates the longitudinal phase spaces of the proton, deuteron, and argon beams at the RFQ entrance point. The DGB was optimized such that the length of the pulsed beam reached a minimum at the RFQ entrance. The main simulation results are summarized in table 2. Here,

Table 1. Beam dynamics simulation settings. The initial current values listed here correspond to approximately the maximum beam currents allowed without de-bunching by space charge effect.

	Proton (A/q = 1/1)	Deuteron (A/q = 2/1)	Argon (A/q = 40/9)
Initial Energy	10 keV/u	10 keV/u	10 keV/u
Initial Emittance (π.mm.mrad)	0.12	0.12	0.12
Initial Current	100 euA	200 euA	400 euA
Chopper Voltage	250 V	500 V	1000 V
Chopper Frequency	100 kHz	100 kHz	100 kHz
Slit (Collimator) Aperture	4 mm	4 mm	4 mm
Switching Time	25 ns	25 ns	25 ns
Buncher Frequency	2 MHz	2 MHz	2 MHz
Buncher Voltage	625 V	1250 V	2500 V

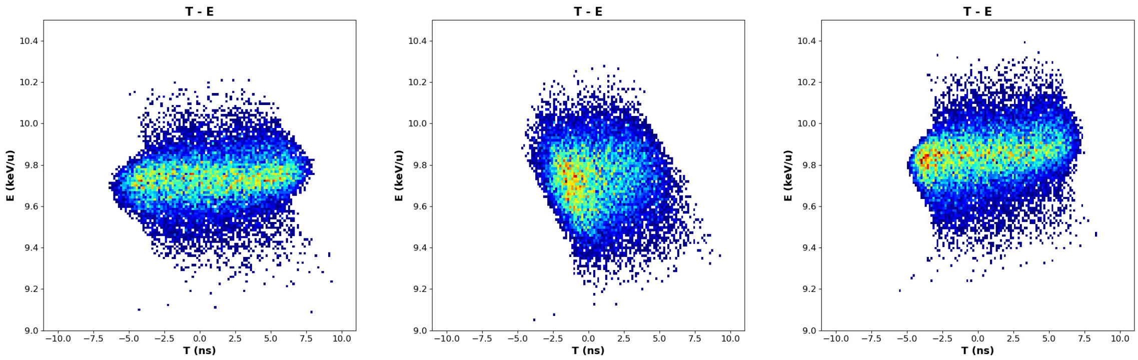

(a) **(b)** **(c)**

Figure 7. Matching simulation results. The longitudinal phase spaces of the (a) proton, (b) deuteron, and (c) argon beams are plotted for the RFQ entrance point.

Table 2. Beam parameters at the RFQ entrance.

	Proton (A/q = 1/1)	Deuteron (A/q = 2/1)	Argon (A/q = 40/9)
Bunch Charge	2.14 pC	3.38 pC	9.50 pC
Emittance X (π.mm.mrad)	0.072	0.101	0.088
Emittance Y (π.mm.mrad)	0.161	0.124	0.151
Pulse Length (98%)	11.3 ns	9.23 ns	10.89 ns

2022 JINST 17 T07007

we define the pulse length as the time duration that covers 98% of the beam particles. At the RFQ entrance, the pulse length of the beam becomes shorter than 12.3 ns (i.e., one RFQ cycle) in all cases. Note that the initial pulse length of the selected beam is approximately 100 ns after the chopper and collimator. In the regular operation without DGB, the bunch charges per one RFQ cycle are 1.23 pC, 2.46 pC, and 4.92 pC for proton, deuterium, and argon beams, respectively. After the bunching process, the bunch charge almost doubles. The increase of the bunch charge provides a higher neutron flux at the target, which is beneficial to users. If an even higher bunch charge is required, the slit width of the collimator would be adjusted.

Ideally, we expect that the pulsed beam is captured in one RF bucket, and a single isolated bunch is generated after the RFQ. However, when the beam particles have a sufficiently large energy spread, neighboring bunches can be generated. Some of the particles with large energy spread would not be captured in the RF bucket and become lost. Table 3 shows RAON's RFQ transmission rate according to the input beam energy spread. The designed transmission rate is 98.4%. Even if energy spread rises up to ±6%, the transmission rate does not decrease dramatically. We note that

Table 3. RFQ transmission rate depending on the energy spread of input beam.

Beam Energy Spread	RFQ Transmission
Design (monoenergetic)	98.4%
± 2%	98.2%
± 4%	98.1%
± 6%	94.9%
± 8%	85.2%
± 10%	76.5%

the RAON RFQ has been designed to have a large acceptance for the input beam energy spread. Nevertheless, some particles may move along the separatrix of the RF bucket and eventually be captured in neighboring RF buckets. In the LEBT simulation, we obtain a selected beam pulse with a pulse length of less than one RFQ cycle. However, the beam acquires a few percent of relative energy spread. To verify the degree of neighboring bunch contamination, we performed an RFQ simulation using the TRACK code.

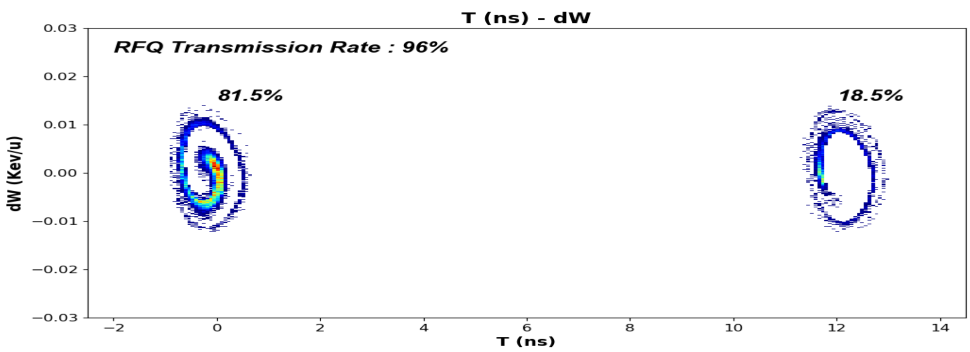

Figure 8. RFQ simulation result for proton beam.

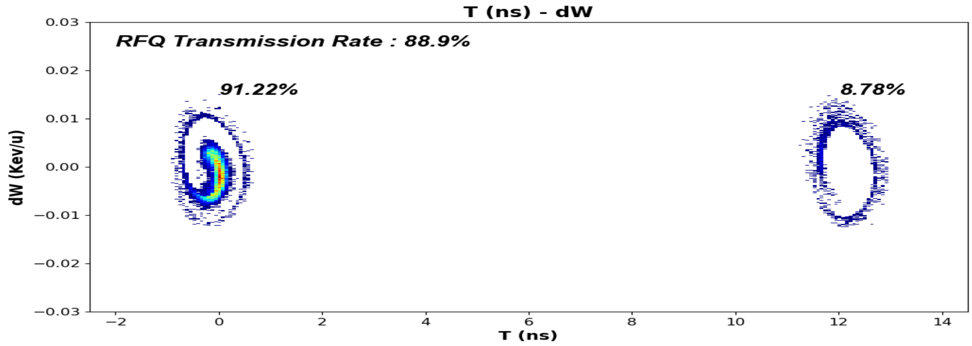

Figure 9. RFQ simulation result for deuteron beam.

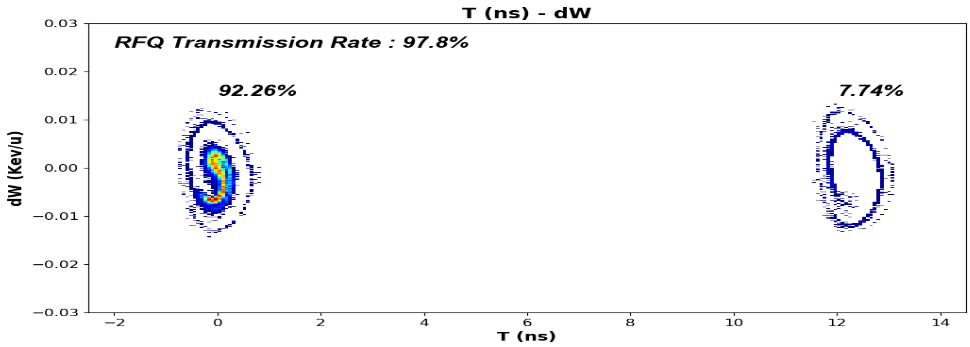

Figure 10. RFQ simulation result for argon beam.

Figures 8, 9, and 10 show the RFQ simulation results for proton, deuteron, and argon beams, respectively. Simulations indicate that the satellite bunches are unavoidable after the RFQ acceleration. The levels of neighboring bunch contamination (i.e., the fraction of satellite bunches with respect to the total beam) are 7.74% and 8.78% for argon and deuteron beams, respectively, which are within the acceptable range for other TOF experiments [2]. For the proton beam, we were not able to maintain a neighboring bunch contamination of less than 15%, mainly because of the higher space-charge effect present in the LEBT. It is anticipated that a more systematic optimization of the initial beam parameters and operating conditions will further improve the single bunch characteristics of the system. It should be noted that, in our RFQ simulations, we assumed that the time delay between the chopper and RFQ is adjusted in such a way that the beam pulse is captured in only two RF buckets.

5 Hardware design and installation

The hardware for the RAON single bunch selection system consists of four main equipment. The first is a high voltage (HV) fast switching system that includes an HV power supply, HV fast switch, and associated electric circuit. The system aims to attain rise/fall times of tens of ns with a maximum voltage of 5 kV at a repetition rate of several hundred kilohertz. A charging/discharging circuit is designed to achieve the required specifications, as shown in figure 11. Here, V1 (V2) is the HV power

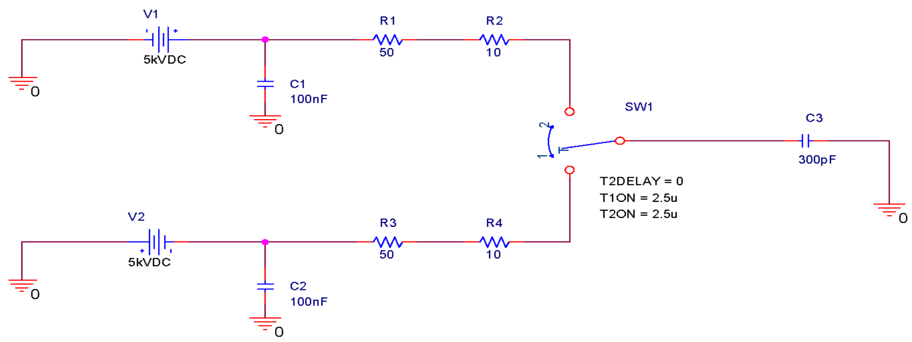

Figure 11. Schematic of the fast HV switching circuit.

supply for a positive (negative) potential and SW1 is the push-pull HV switch commercially available from BEHLKE. Buffer capacitors C1 and C2 are adjusted to maintain voltage stability and ensure a fast rise/fall time. Capacitive load C3 represents the capacitance of the chopper electrodes, including the cable capacitance and extra stray capacitance in the system. The capacitance of the chopper electrodes was measured to be approximately 66 pF. Thus, we estimated that the total capacitance of the system may be below 100 pF. Nevertheless, to allow some margin for the stray capacitance of the system (including switch output capacitance), we set C3 to 300 pF in our design study.

The required repetition rate of a single bunch is usually determined by the TOF experiments. For RAON, the required repetition rate ranges between 100–200 kHz. To meet the repetition rate requirement and ensure a switching time of less than 100 ns (as discussed in section 3), we use HTS-201-20 GSM (HFS, DLC option) made by BEHLKE. For the HV power supply, we use LH5R1.0 from XP Power, which has a maximum current of 1 A. In our switching circuit, the HV power supply must rapidly (i.e., within one repetition cycle) recharge the buffer capacitance. We did circuit simulations for the schematic shown in figure 11, and confirmed that we need power supplies which have sufficient currents. If the current from the power supply is insufficient, the buffer capacitance charge decreases continuously, which is problematic for long-term operation with a high repetition rate. Figures 12 and 13 demonstrate this characteristic. The required current

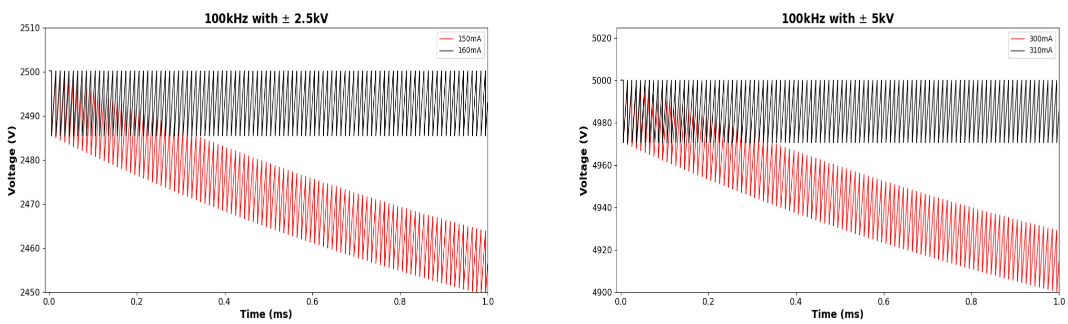

Figure 12. Buffer capacitor voltage for 100 kHz repetition rate with ±2.5 kV (left) and ±5 kV (right) operations.

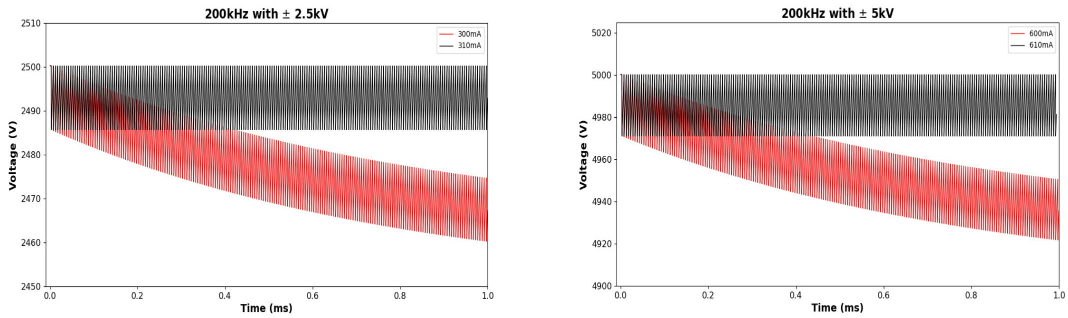

Figure 13. Buffer capacitor voltage for 200 kHz repetition rate with ±2.5 kV (left) and ±5 kV (right) operations.

for 100 kHz repetition rate and ±2.5 kV operation is predicted to be around 150–160 mA. When we apply 150 mA current setting to the simulation, the buffer capacitor cannot be recharged in one repetition cycle. Hence, the voltage of the buffer capacitor decreases with reducing the maximum chopper voltage. Other simulation cases show a similar behavior. For the most harsh condition (200 kHz repetition rate and ±5 kV operation), we need current more than 600 mA. In the circuit simulation, we assumed an ideal constant-current source, but in reality, it may be not. Therefore, we set some margin, and chose a power supply with a maximum current of 1 A, which should be sufficient to avoid such a problem.

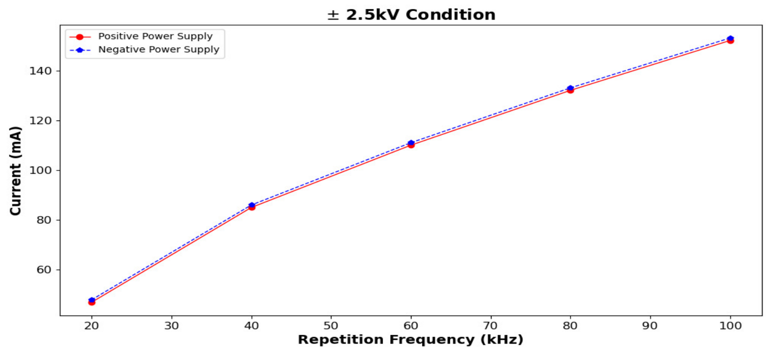

Figure 14. Actual current consumption at the fast chopper power supplies.

Figure 14 shows the current consumption at the chopper power supplies. We tested at the repetition frequencies of 20, 40, 60, 80, and 100 kHz with ± 2.5 kV. The maximum current consumption was around 150mA. Figure 15 shows the vacuum chamber housing the chopper electrodes installed in the LEBT section. The collimator will be installed horizontally through the vacuum ports. Figure 16 shows the electronics of the fast chopper. The yellow box at the top is an electric circuit with an HV fast switch of BEHLKE. The two pieces of equipment at the bottom are HV power supplies. One is for the negative, and the other is for the positive voltage. Figures 17 and 18 present the experimental results of the HV fast switch. We verify the rise/fall time of the entire system. The repetition rate of the switch was 100 kHz, and the voltage of the HV power supply was ±2.5 kV. In figures 17 and 18, the voltage range is −2.5 ∼ +2.5 V because we use a

2022 JINST 17 T07007

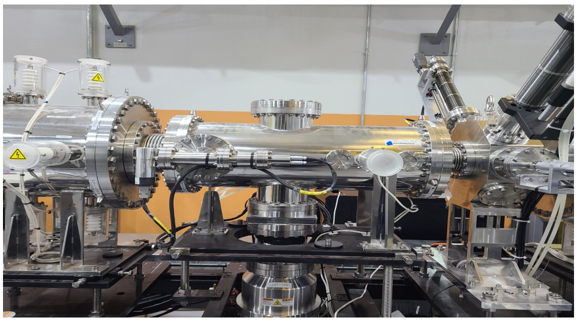

Figure 15. Vacuum chamber housing the chopper.

Figure 16. Rack for the chopper electronics.

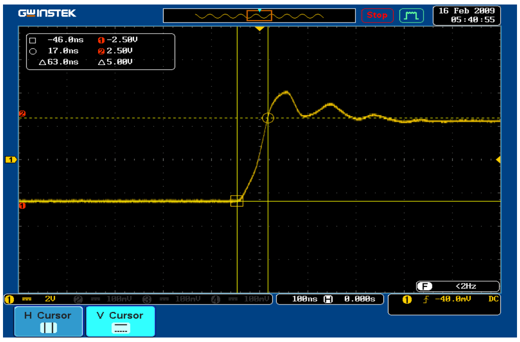

Figure 17. Chopper rise time ie measured between the 0% and 100% signal voltage levels.

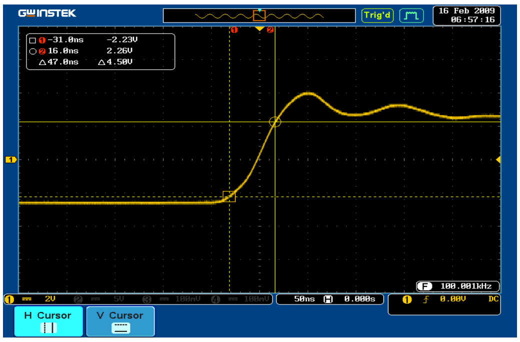

Figure 18. Chopper rise time ie measured between the 10% and 90% signal voltage levels.

1000:1 attenuating high voltage probe. The chopper rise time between the 0% and 100% signal voltage levels is 63 ns, and that for the 10% and 90% signal voltage levels is 47 ns. As discussed previously, our goal was to achieve a rise time under 100 ns. Therefore, we confirmed that the HV fast switch works properly in an actual setting. Some overshoots appeared in the voltage waveforms but they do not affect the overall chopping process.

The second piece is a slit-type collimator system, which is used as a beam dump. Because we must deal with various A/q beams, the slit width must be adjustable. Figure 19 presents the 3D CAD drawing of the collimator. We made two sets of collimators, which are installed on both sides of the vacuum chamber as shown in figure 20. The maximum slit width is 70 mm, which is sufficiently large that the beam particles are not influenced during normal operation. The slit plate is made of stainless steel. The maximum power at the collimator is approximately 10 W; thus, water cooling was not essential. However, we decided to apply water cooling to suppress possible outgassing by heating.

The third one is the double gap buncher (DGB). It has a central electrode and two ground electrodes (see figure 21). The planned RF frequency of the DGB is 2 MHz and a maximum 5 kV RF voltage will be applied to the central electrode. When the beam arrives at the DGB, the pulse length is approximately 150 ns. To apply bunching for a 150 ns pulse length beam, the bunching frequency must be below 3 MHz because of the longitudinal acceptance. To allow for some margin in the pulse length, we set the nominal frequency to 2 MHz.

The length of the central electrode is 270 mm, which is set according to $\frac{0.8\pi}{2.0\pi} \times \beta\lambda$. Here, $\beta(= 0.0046)$ is the relativistic parameter and λ is the RF wavelength. This is not the optimal value

2022 JINST 17 T07007

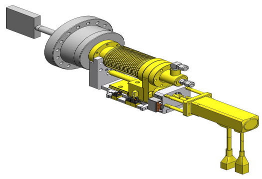

Figure 19. 3D CAD drawing of the collimator.

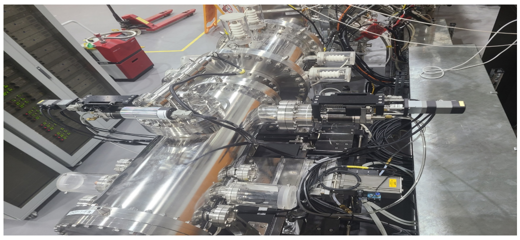

Figure 20. Installed collimator at the chopper vacuum chamber.

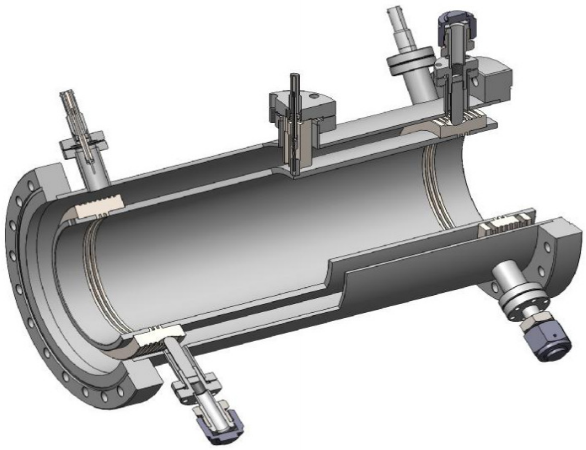

Figure 21. A cutaway drawing of the DGB.

for π mode 2 MHz sinusoidal RF waves. Indeed, the length is optimal for 2 MHz saw-tooth wave with 0.8π phase shift, which leads to a minimal power consumption (based on ref. [4]). In the future, we plan to use a saw-tooth voltage waveform (which is better in terms of voltage linearity) by superposing three sin waves. The gap distance between the central and ground electrodes is 10 mm, and ceramics are used for insulation and mechanical support.

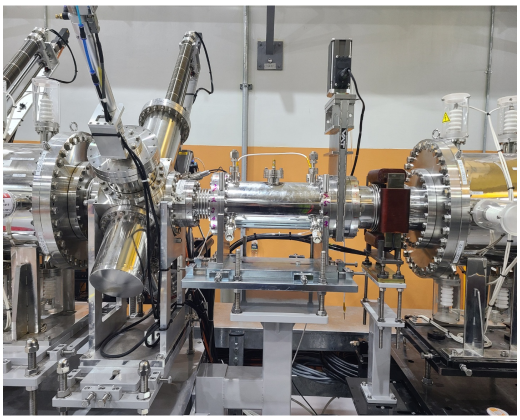

Figure 22. Vacuum chamber housing the DGB.

Figure 23. RF electronics for the DGB.

Figure 22 shows the vacuum chamber housing the DGB installed in the LEBT section. Figure 23 shows the RF electronics used in the DGB, in which the bottom piece is the RF amplifier manufactured by Tomco (model BT00100-Alphas-CW-1000 with a maximum power of 1 kW), and the top box is an impedance matching and voltage boosting circuit. The DGB has passed a vacuum leak test, and RF conditioning is in progress.

The last item is the RF system, which consists of an RF signal generator, RF amplifier, and an impedance matching and voltage boosting circuit. The total system boosts the RF voltage to a maximum of approximately 5 kV. Figure 24 shows the simplified schematic of the RF system. If

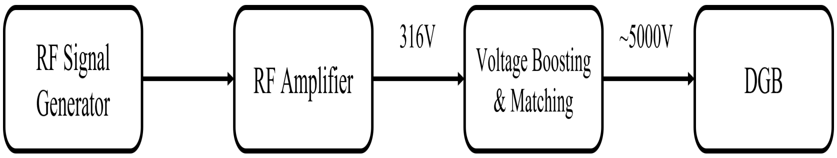

Figure 24. Schematic of the DGB RF system.

the system is ideally matched to 50 Ω, the maximum output voltage from the 1-kW RF amplifier would be approximately 316 V. Because we need up to 5 kV of DGB voltage to cover various heavy ion beams, we designed a dedicated impedance matching and voltage boosting circuit. Figure 25

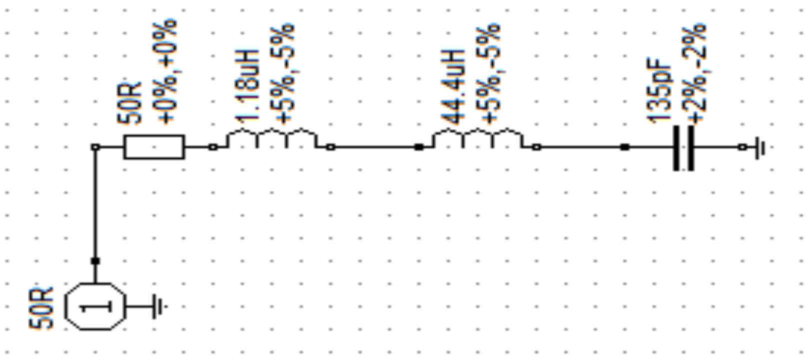

Figure 25. Circuit diagram of the impedance matching and voltage boosting circuit.

presents a schematic of the impedance matching and voltage boosting circuit. The voltage generator on the left represents the RF amplifier with signal generator, and the 135-pF capacitor on the right represents the DGB. The capacitance of DGB is not a fixed value and it can be changed by actual experiment environment. The 50 Ω resistor and 1.18 μH inductor represent the total impedance of the high power resistor and transformer. Initially, we tried to increase the voltage using an 1:16 turns ratio transformer. However, the circuit did not operate properly because the transformer was not ideal. The transformer has a finite inductance and resistance; therefore, the reactance component deteriorated the entire circuit matching. Therefore, we used a series resonance circuit that could utilize the inductance of the transformer. Eventually, we used a 2:4.5 turns ratio transformer and designed a circuit with a much smaller reactance than that of the DGB. Consequently, the circuit could boost the input voltage by approximately 10–20 times, which is sufficient for our applications.

6 Control system

Many accelerator facilities use EPICS [13] program for their control systems. The central control system of the RAON is also programmed using EPICS. Hence, we adopted EPICS so that the local control system can be smoothly integrated into the RAON central control. Figure 26 shows a schematic of the control system utilized in the RAON single bunch selection system. The local EPICS input-output controller (IOC) runs on a Raspberry Pi and is connected to the RAON main control network.

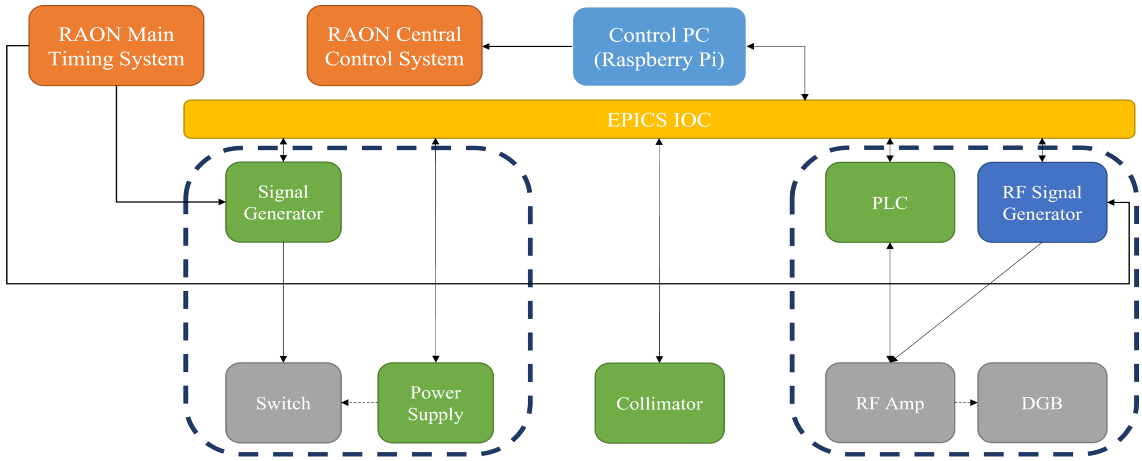

Figure 26. Schematic of the control system.

Timing synchronization is achieved by the RAON central timing system and T560 delay generator. The main timing system of the RAON can produce 3.3 V or 5 V TTL pulse. Furthermore, the minimum controllable time is 12.3 ns, which is sufficient for synchronizing the DGB and RFQ. However, this is not sufficient for the fast chopper because the beam energy after the chopper can be changed to an arbitrary value. The timing system must control the trigger within a few ns to synchronize the chopper system properly. Therefore, we use the T560 delay generator for fine-tuning. Figure 27 shows the screen capture of the control GUI created using a control system studio (CSS) [14]. The collimator and high voltage power supply control panels are placed on the left-hand side, and the RF signal generator and amplifier can be controlled using the right-hand side panel. The bottom panel is for the delay generator that will be used for fine tuning the timing synchronization.

7 Summary

Several single-bunch selection methods have been proposed and tested for accelerator-based TOF experiments worldwide. However, the direct application of one of these methods to the RAON accelerator is not straightforward owing to several constraints. Therefore, we developed a scheme that combines SARAF's fast chopper and TRIAC's DGB methods. Through simulations, we confirmed that we could create a single isolated bunch after RFQ acceleration with an acceptable amount of satellite bunches. Controlling the neighboring bunch contamination will be further optimized in future studies.

2022 JINST 17 T07007

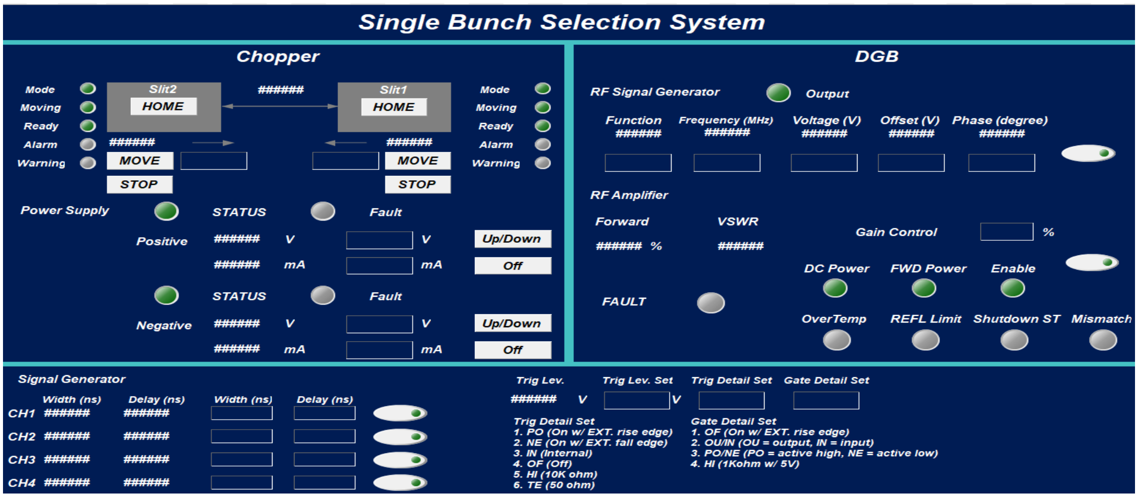

Figure 27. Control system GUI.

The proposed single bunch selection system for the RAON consists of an HV fast switching system, collimator, DGB, and RF supply system. The HV fast-switching system aims to attain rise/fall times of tens of ns for a maximum input voltage of 5 kV. In the circuit simulations, the rise/fall time of the switching system is estimated to be 58 ns. In the actual experiment, the rise/fall time exhibited a similar value to the simulation result. The DGB has a 2 MHz bunching frequency and can supply a maximum RF voltage of 5 kV. The central electrode length of the DGB was designed to be 270 mm considering the possibility of using a sawtooth voltage waveform. The 1-kW RF amplifier can generate a maximum voltage of 316 V with a 50 Ω impedance matching circuit. This maximum voltage is too low for our application; therefore, an additional transformer and serial resonance circuit were applied for voltage boosting.

The operation scenario optimization is undergoing. Further improvements in minimizing the neighboring bunch contamination and maximizing the repetition rate will be actively pursued.

Acknowledgments

This work was supported by the National Research Foundation (NRF) of Korea (Grant No. NRF-2020R1A2C1010835). This work was also supported by the Rare Isotope Science Project of the Institute for Basic Science funded by the Ministry of Science and ICT (MSIT) and the NRF of Korea under Contract 2013M7A1A1075764.

References

[1] A. Shor et al., *Fast beam chopper at SARAF accelerator via RF deflector before RFQ*, 2012 *JINST* **7** C06003.

[2] A. Shor et al., *Fast chopper for single radio-frequency quadrupole bunch selection for neutron time-of-flight capabilities*, *Phys. Rev. Accel. Beams* **22** (2019) 020403.

2022 JINST 17 T07007

[3] P. Dolegieviez, R. Ferdinand, X. Ledoux, H. Savajols and F. Varenne, *Status of the SPIRAL2 project*, in *Proceedings of the* 10^{th} *Int. Particle Accelerator Conf.* **IPAC2019**, Melbourne, Australia, 19–24 May 2019, JACOW Publishing, Geneva, Switzerland (2019), p. 844.

[4] M. Okada et al., *Low-background prebunching system for heavy-ion beams at the Tokai radioactive ion accelerator complex*, *Phys. Rev. ST Accel. Beams* **15** (2012) 030101.

[5] N. Inabe, M. Kase, I. Yokoyama, A. Goto and Y. Yano, *Development of a single-bunch selector for the RIKEN ring cyclotron*, Tech. Rep. JAERI-Conf 95-021, (1995).

[6] J.H. Kim and Y.S. Kim, *Simulation study of a double-gap particle buncher for low-energy protons*, *J. Korean Phys. Soc.* **61** (2012) 189.

[7] M. Di Giacomo et al., *Proton beam commissioning of the SPIRAL2 single bunch selector*, 2020 *JINST* **15** T12011.

[8] Y.K. Kwon et al., *Status of rare isotope science project in Korea*, *Few-Body Syst.* **54** (2013) 961.

[9] K. Tshoo et al., *Experimental systems overview of the rare isotope science project in Korea*, *Nucl. Instrum. Meth. B* **317** (2013) 242.

[10] *Warp webpage*, http://warp.lbl.gov/.

[11] *TraceWin rapid explanation*, http://irfu.cea.fr/en/Phocea/Page/index.php?id=780.

[12] *TRACK webpage*, https://www.phy.anl.gov/atlas/TRACK/.

[13] *EPICS webpage*, https://epics.anl.gov.

[14] *Control System Studio webpage*, https://controlsystemstudio.org/.